

# Increased Amazon basin wet-season precipitation and river discharge since the early 1990s driven by tropical Pacific variability



ENVIRONMENTAL RESEARCH
LETTERS

**ACCEPTED MANUSCRIPT • OPEN ACCESS**

# Increased Amazon basin wet-season precipitation and river discharge since the early 1990s driven by tropical Pacific variability

To cite this article before publication: Andrew R. Friedman *et al* 2020 *Environ. Res. Lett.* in press https://doi.org/10.1088/1748-9326/abd587

# Increased Amazon basin wet-season precipitation and river discharge since the early 1990s driven by tropical Pacific variability

Andrew R. Friedman[1,2], Massimo A. Bollasina[1], Guillaume Gastineau[3], and Myriam Khodri[3]

[1] University of Edinburgh, School of Geosciences, Edinburgh, United Kingdom

[2] Institute of Geography and Oeschger Centre for Climate Change Research, University of Bern, Switzerland

[3] Laboratoire d'Océanographie et du Climat : Expérimentations et Approches Numériques (LOCEAN), Pierre and Marie Curie / Sorbonne University: Paris, France

Resubmission to *Environmental Research Letters*, November 2020

Corresponding author: Andrew R. Friedman. <andrew.friedman@ed.ac.uk>
ORCID ID: https://orcid.org/0000-0001-6994-2037

## Abstract

The Amazon basin, the largest watershed on Earth, experienced a significant increase in wet-season precipitation and high-season river discharge from the early 1990s to early 2010s. Some studies have linked the increased Amazon hydrologic cycle to decadal trends of increased Pacific trade winds, eastern Pacific SST cooling, and the associated strengthening of the Walker circulation. However, it has been difficult to disentangle the role of Pacific decadal variability from the impacts of greenhouse gases and other external climate drivers over the same period. Here, we separate the contributions of external forcings from those of teleconnections from Pacific decadal variability by comparing two large ensembles of climate model experiments with identical radiative forcing agents but imposing different tropical Pacific wind stress. One ensemble constrains tropical Pacific wind stress to its long-term climatology, suppressing tropical Pacific decadal variability; the other ensemble imposes the observed tropical Pacific wind stress anomalies, simulating realistic tropical Pacific decadal variability. Comparing the Amazon basin hydroclimate response in the two ensembles allows us to distinguish the contributions of the external forcings common to both simulations from those related to the Pacific trade wind variability. For the 1992–2012 trend, we find that the experiments with applied observed tropical Pacific wind stress anomalies simulate the strengthened Walker circulation between the Pacific and South America, sharpened Pacific–Atlantic interbasin contrast in sea surface temperature, and increased Amazon basin wet-season precipitation and high-season discharge. These strengthened Walker circulation and Amazon hydrologic intensification trends are absent in the simulations with applied climatological tropical Pacific wind

stress. This work underscores the importance of Pacific decadal variability in driving hydrological cycle changes and modulating the hydroclimate impacts of global warming over the Amazon basin.

## 1. Introduction

The Amazon river is by far the Earth's largest river by flow, responsible for 15–20% of the freshwater discharged into the oceans (Molinier et al., 1996; Dai et al., 2009). Its basin holds the largest planetary watershed and rainforest, which play key roles in the global climate system and carbon cycle and contain a wealth of biodiversity (Foley et al., 2002; Malhi et al., 2008). Recent extensive dry-season droughts and fires have heightened concerns about climate change and deforestation (Nobre et al., 2016; Marengo et al., 2018). Additionally, starting in the early 1990s, the Amazon basin experienced a dramatic increase in wet-season (December–May) precipitation, resulting in an overall strengthening of the hydrological cycle, heightened peak river discharge, and highly disruptive flood events (Gloor et al., 2013, 2015; Marengo and Espinoza, 2016; Barichivich et al., 2018). The increased discharge also reduced the tropical Atlantic surface salinity (Gouveia et al., 2019), with potential impacts on ocean circulation and large-scale climate (Jahfer et al., 2017). Understanding the drivers and mechanisms of this recent Amazon hydrological intensification is important for assessing the uncertainties associated with climate change projections.

The Amazon hydrological cycle intensification coincided with a pronounced climatic shift in the tropical Pacific. Over the 20-year period beginning in the early 1990s, there was an unprecedented strengthening of the Pacific trade winds compared to previous decades (Balmaseda et al., 2013; de Boisséson et al., 2014). This was associated with SST cooling in the equatorial central and eastern Pacific, which was reflected in a reduced rate of global surface temperature increase compared to previous decades, sometimes referred to as the *hiatus* (Kosaka and Xie, 2013; Meehl et al., 2011). The trade wind and SST changes were connected to a strengthening of the Pacific Walker circulation and more frequent La Niña phases of the El Niño / Southern Oscillation (ENSO) (Dong and Lu, 2013; Liu and Zhou, 2017). On decadal timescales, these trends reflected a transition from the warm to the cold phases of the Interdecadal Pacific Oscillation (IPO; Power et al., 1999; Zhang et al., 1997), with a larger amplitude than previous transitions in the instrumental record (England et al., 2014).

Observational analysis has connected the increased Amazon precipitation from the early 1990s to the Pacific trade wind strengthening, SST cooling, and intensified Walker circulation (Barichivich et al., 2018), building on well-established ENSO teleconnections in the tropics (Ropelewski and Halpert, 1987; Dai and Wigley, 2000). However, it is difficult using observations alone to separate

the influence of Pacific variability on Amazon precipitation from that of greenhouse gases (GHGs) and other external climate forcing agents over the same period; as such, climate model sensitivity experiments can be useful to shed light on and disentangle the contemporaneous impacts of different drivers (Hegerl and Zwiers, 2011).

In this study, we use a set of companion large-ensemble climate model simulations with tropical Pacific surface wind stress nudging. The two experiments have identical external forcing agents but impose different surface wind stress regimes in the tropical Pacific, while allowing the climate system to evolve freely outside the tropical Pacific. In the first ensemble, W-CLIM, the tropical Pacific wind stress is constrained to its long-term climatological values, thus simulating the counterfactual trajectory of the climate system holding a fixed neutral IPO state. In the second ensemble, W-FULL, the observed wind stress anomalies are imposed in the tropical Pacific. W-FULL thus simulates the evolution of the climate system with realistic tropical Pacific decadal variability, including the IPO phase transition and the trade wind acceleration from the early 1990s. By comparing the Amazon basin hydroclimate response in W-CLIM and W-FULL, we can distinguish the contributions of the external forcings common to both simulations from those related to the Pacific trade wind variability found only in W-FULL.

## 2. Methods and data

We examine a set of experiments with the IPSL-CM5A-LR global climate model (Dufresne et al., 2013). Its atmospheric component is LMDZ5A (Hourdin et al., 2013), with a resolution of 3.75° × 1.875° and 39 vertical levels. The land surface component is ORCHIDEE (Krinner et al., 2005), with a similar horizontal resolution as the atmosphere; and the ocean component is NEMOv3.2 (Madec, 2008). The experimental setup, further described in Gastineau et al. (2019), consists of two 30-member ensembles, each initialized in 1979 from a spread of random phases of the IPO and the Atlantic Multidecadal Oscillation (AMO) (Kerr, 2000) from the IPSL-CM5A-LR fully-coupled historical large ensemble (Frankignoul et al., 2017). Both ensembles are forced by identical Fifth Coupled Model Intercomparison Project (CMIP5) historical and Representative Concentration Pathway 8.5 (RCP8.5) GHG and ozone emissions from 1979–2014 (Taylor et al., 2012). Volcanic aerosols are included, but anthropogenic aerosols are fixed at 1940 values in both experiments.

In both ensembles, surface wind stress ($\tau$) is prescribed in the ocean component in the tropical Pacific from 20°S to 20°N with a buffer region from 15°–25° latitude (outlined in **Fig. 1a**), while leaving the climate system unconstrained outside the tropical Pacific. Prescribing wind stress tightly constrains SST through its effects on zonal advection, thermocline depth, and eastern Pacific

upwelling (Clarke, 2008). It is somewhat similar to nudging SST (Kosaka and Xie, 2013; McGregor et al., 2014), but favors the dynamical consistency between the atmosphere and ocean, and reduces artificial heat fluxes imposed into the ocean (Douville et al., 2015; Watanabe et al., 2014). In the representative climatological ensemble, W-CLIM, the 1979–2014 climatological wind stress from the IPSL-CM5A-LR historical and RCP8.5 CMIP5 ensemble mean is prescribed, with additional model noise to deepen the mixed layer; this is further described in **Text S1**. W-CLIM thus does not simulate the variability resulting from tropical Pacific wind stress changes.

In the second ensemble, W-FULL, daily wind stress anomalies from 1979–2014 from the ECMWF ERA-Interim Reanalysis (hereafter ERA-I; Dee et al., 2011) are added to the model climatology and prescribed in the ocean model component.. **Fig. 1a** shows the 1992–2012 ERA-I mean $\tau$ trend over the nudging region during the Amazon wet season (December–May). **Fig. 1b** shows the corresponding zonal wind stress ($\tau_x$) anomaly over the Niño 4 region (160°E–150°W, 6°S–6°N) from ERA-I and applied in W-FULL, illustrating the significant ($p$<0.05) strengthening trend from1992–2012. An error in the treatment of the ERA-I $\tau$ anomalies induced $\tau$ amplitudes about 20% larger in W-FULL than ERA-I, though the overall interannual changes are very similar and the spatial patterns are identical (Gastineau et al., 2020).

For precipitation, we examine the monthly 2.5° × 2.5° combined satellite-gauge Global Precipitation Climatology Project (GPCP), version 2.3 (Adler et al., 2003, 2018). We take December–May as the Amazon basin-wide wet season, which is associated with the South American monsoon system, while recognizing that the seasonal cycle varies regionally within the basin (Marengo et al., 2012; Wang et al., 2018). IPSL-CM5A-LR generally reproduces the observed wet-season regional precipitation climatology (**Figs. S1a-S1c**). In common with many CMIP5 models, it suffers from a double intertropical convergence zone (ITCZ) in the eastern Pacific (Jones and Carvalho, 2013; Li and Xie, 2014); there is also excessive precipitation over the Andes relative to the Amazon basin interior (Dufresne et al., 2013). IPSL-CM5A-LR effectively simulates the observed seasonal cycle of Amazon region mean precipitation (**Fig. S1d**), though similar to many CMIP5 models, it underestimates overall Amazon precipitation, particularly during the July-October dry season (Yin et al., 2013).

To complement precipitation, we examine monthly Amazon discharge (in $m^3\ s^{-1}$) from the farthest downstream long-term gauge at Óbidos (55.7°W, 1.9°S; indicated in **Fig. 2a**), which captures runoff from most of the basin (Dai and Trenberth, 2002). River discharge provides an integrated measure of Amazon basin hydroclimate, though it does not allow us to differentiate between recirculated and non-recirculated precipitation (Gloor et al., 2013; Dai, 2016). For the model, we use

the output of freshwater flux into the ocean from rivers (in kg $m^{-2}$ $s^{-1}$) multiplied by the respective gridcell area to obtain a monthly volume flux, which we integrate over the Amazon outflow region (45°–51°W, 2°S–6°N; blue box in **Figs. 2b-2c**).

In observations, the 1980–1992 mean seasonal cycle of Amazon discharge (**Fig. S1e**) shows a gradual increase peaking in May and June. Óbidos discharge lags basin-average precipitation by around three months due to the time for surface runoff to travel downstream (Dai and Trenberth, 2002; Marengo, 2005). The model seasonal discharge maximum arrives 1-2 months early, peaking in April, and lasts for a shorter period compared to observations, which reflects ORCHIDEE deficiencies over the Amazon region (Guimberteau et al., 2012, 2014) and its floodplain storage not being activated in the CMIP5 experiments (Agnès Ducharne, personal communication). To allow for comparison between observations and simulations given the annual cycle phase differences, we track the high-season discharge by taking the mean of the five largest-discharge months of each year (with the discharge year spanning from February–January). In addition to precipitation and discharge, we use the monthly 2°×2° NOAA Extended Reconstructed SST dataset (ERSST), version 5 (Huang et al., 2017), as well as monthly 2.5° × 2.5° atmospheric fields from ERA-I.

Our analysis focuses on the Amazon wet season, for which the tropical Pacific has relatively greater influence on interannual variability (Yoon and Zeng, 2010; Andreoli et al., 2012), over the 21-year trend from 1992–2012, corresponding to the maximum Pacific trade wind strengthening (Balmaseda et al., 2013; de Boisséson et al., 2014). Trend significance is calculated based on a 2-tailed Student's *t*-test of the slope, adjusting the standard error and degrees of freedom assuming a first-order autoregressive (AR1) noise model (Santer et al., 2000). We also examine interannual correlations of linearly-detrended time series over the entire 1980–2014 period, with significance evaluated based on a 2-tailed Student *t*-test, adjusting the degrees of freedom assuming an AR1 noise model (Bretherton et al., 1999). We describe trends and correlations as significant when $p<0.05$. The W-CLIM and W-FULL ensemble means are analyzed in order to emphasize the robust signals in each experiment.

## 3. Results

### *3.1 Precipitation and discharge trends*

The 1992–2012 observed wet-season precipitation trend (**Fig. 2a**) is positive over the Amazon and northern South America extending into the equatorial Atlantic. In the eastern Pacific, it is positive from 5°–10°N and negative along the equator. W-FULL (**Fig. 2b**) well reproduces the spatial pattern and magnitude of the observed trend, though the precipitation increase in South America is shifted to

the south, with some drying in the northern Amazon. W-FULL also overestimates the positive trend in the equatorial Atlantic and the negative trend in the eastern equatorial Pacific. W-CLIM (**Fig. 2c**), which has much smaller amplitudes (note different color scale), shows wettening in the eastern equatorial Pacific contrasting with drying in the western Amazon, and a weaker precipitation increase in the eastern Amazon extending into the equatorial Atlantic.

**Fig. 2d** shows the observed and simulated wet-season mean precipitation anomaly averaged over the Amazon region (75°–50°W, 12.5°S–5°N) and respective 1992–2012 linear trends. W-FULL reproduces the significant positive 1992–2012 trend found in observations (**Table 1**). It also captures much of the observed interannual variability, with a significant correlation with GPCP (**Table 2)**. The mean 5-month high-season Amazon river discharge is shown in **Fig. 2e**. Like precipitation, W-FULL captures the 1992–2012 positive trend and is significantly correlated with Óbidos observations. W-CLIM lacks a discernible trend in basin-wide precipitation or discharge.

*3.2 SST and atmospheric circulation*

The 1992–2012 trends in relative SST and low-level atmospheric circulation are shown in **Figs. 3a-3c.** Relative SST (referred to as SST*), the deviation from the tropical mean (20°S–20°N) SST, captures the spatial gradients of SST and low-level moisture which are important for tropical convection (Vecchi and Soden, 2007; Ma and Xie, 2013; Khodri et al., 2017); absolute SST is shown in **Fig. S2**. ERSST (**Fig. 3a**) features SST* cooling in the tropical central and eastern Pacific resembling the pattern associated with the transition from positive to negative IPO phases, with equatorial SST* cooling extending into both hemispheres along the eastern boundary; and SST* warming in the tropical Atlantic. W-FULL (**Fig. 3b**) shows a similar pattern, though with larger-amplitude equatorial Pacific SST* cooling and without extending toward the mid-latitudes. These differences may reflect the larger-amplitude $\tau$ anomalies applied (Gastineau et al., 2020) or model cold tongue SST and double ITCZ biases (Li and Xie, 2014; Bellenger et al., 2014). In contrast, W-CLIM (**Fig. 3c**) shows equatorial Pacific SST* warming, as expected from global warming processes found in coupled models (DiNezio et al., 2009). ERA-I and W-FULL feature increased 850-hPa winds into the Amazon region from the tropical North Atlantic, one of the key pathways for Amazon climatological moisture convergence (Grimm, 2003; Arraut et al., 2012).

**Fig. 3d** presents variations of the Pacific–Atlantic interbasin SST contrast (Pac–Atl $\Delta$SST), which reflects the strength of the Walker circulation (Wang, 2006; McGregor et al., 2014; Chikamoto et al., 2015) and has been linked to wet-season Amazon precipitation (Gloor et al., 2015; Barichivich et al., 2018). Pac–Atl $\Delta$SST is calculated as the difference between the tropical central and eastern

Pacific (180°–90°W, 10°S–10°N) and the tropical Atlantic (40°W–15°E, 10°S–10°N; boxes in **Figs. 3a-3c**). We find that Pac–Atl ΔSST is significantly negatively correlated with Amazon wet-season precipitation and river discharge in observations and the simulations (**Table S1**). Consistent with the precipitation and discharge trends, W-FULL captures the significant 1992–2012 observed negative Pac–Atl ΔSST trend (**Table 1**). Though ERSST has greater tropical North Atlantic SST* warming and W-FULL has greater tropical South Atlantic SST* warming, this discrepancy is not reflected in Pac–Atl ΔSST. The W-CLIM Pac–Atl ΔSST trend is an order of magnitude smaller and of opposite sign.

In order to more clearly identify the zonal circulation changes, we examine the trends in pressure vertical velocity (ω) and the zonal component of the divergent wind ($u_{div}$) averaged over the maximum precipitation trend signal over the Amazon latitudes (0–10°S; **Fig. 4)**. ERA-I and W-FULL feature increased ascent over the Amazon region and weakened ascent over the central equatorial Pacific (**Figs. 4a-4b**), depicting strengthening of the climatological Walker circulation branch between the Pacific and South America (Dong and Lu, 2013; Liu and Zhou, 2017). In contrast, W-CLIM features a small weakening of the ascent over the western Amazon region (**Fig. 4c**), consistent with the weakening of the Walker circulation expected from global warming (Vecchi and Soden, 2007). The meridional circulation, depicted through ω and the meridional component of the divergent wind ($v_{div}$) zonally averaged from 75–50°W (**Fig. S3**), also reveals enhanced Amazon uplift in ERA-I and W-FULL, though displaced to the south in W-FULL.

*3.3 Moisture convergence*

We next examine moisture convergence, which is the predominant contributor to Amazon basin wet-season precipitation and the leading driver of its interannual variability (Angelini et al., 2011; Drumond et al., 2014; Satyamurty et al., 2013b). Following Satyamurty (2013a, 2013b), we also integrate the moisture fluxes across the four Amazon region boundaries. ERA-I and the simulations feature climatological wet-season moisture convergence over the Amazon region (**Table S2a, Fig. S4,**). Consistent with the precipitation and discharge increases, ERA-I and W-FULL have significant positive moisture convergence trends over the Amazon region from 1992–2012 (**Table S2b, Fig. S5**). However, the increased convergence is mostly due to northeasterly moisture advection from the tropical North Atlantic in ERA-I, while W-FULL simulates increased westerly moisture flux from the equatorial Pacific.

We additionally use the linear approximation of Huang (2014) to elucidate the separate contributions of dynamics and thermodynamics to the 1992–2012 Amazon region precipitation trend:

$$\Delta P \sim \Delta\omega \cdot \overline{q} \; + \; \overline{\omega} \cdot \Delta q,$$

where P is precipitation; $q$ denotes 925-hPa specific humidity; and $\omega$ is 500-hPa pressure velocity. The dynamic component ($\Delta\omega \cdot \overline{q}$) accounts for nearly all of the Amazon region moisture convergence increase in ERA-I and W-FULL, indicating that atmospheric circulation changes are predominant for the precipitation trend (**Table S3**). In W-CLIM, which has little overall moisture convergence change, the thermodynamic component ($\overline{\omega} \cdot \Delta q$) of increased moisture convergence opposes the reduced dynamic component due to the tropical circulation weakening.

## 4. Discussion

Using a companion set of climate model experiments with identical external forcing agents but differently constrained tropical Pacific wind stress, we attribute the 1992–2012 observed increases in wet-season Amazon basin precipitation and high-season river discharge to the contemporaneous Pacific trade wind strengthening. In the simulations with applied observed tropical Pacific wind stress anomalies (W-FULL), the imposed Pacific trades cause equatorial Pacific SST cooling, sharpening the Pacific–Atlantic zonal SST contrast (Pac–Atl ΔSST) and strengthening the Pacific-South America branch of the Walker circulation. The enhanced central and eastern Pacific subsidence and compensating convergence over the Amazon climatological ascending region lead to increased Amazon wet-season precipitation and high-season discharge (Gloor et al., 2015; Barichivich et al., 2018).

In contrast, the companion experiment with applied climatological tropical Pacific wind stress simulating a neutral IPO state (W-CLIM) does not produce significant changes in Amazon wet-season precipitation or high-season discharge. W-CLIM has a larger 1992–2012 trend in absolute tropical Atlantic SST than W-FULL (**Fig. S2d**), though not in the relative Pac–Atl ΔSST (**Fig. 3d**) which is important for Amazon wet-season convection. While atmosphere-only experiments have shown a strong influence of Atlantic SST warming alone on the Amazon wet-season precipitation increase from 1979–2015 (Wang et al., 2018), these simulations are not directly comparable to our approach since they impose climatological SST outside the perturbed SST basin, whereas we allow ocean-atmosphere feedbacks through interactive air-sea coupling and include the SST evolution resulting from external forcings.

The W-CLIM setup assumes that the tropical Pacific wind stress did not respond to external forcing during the observed strengthening period. This assumption has been challenged by findings that anthropogenic Asian sulfate aerosols contributed to the increased Pacific trade winds (Smith et

al., 2016; Takahashi and Watanabe, 2016), though the linkage has been questioned (Oudar et al., 2018). There is also evidence that the Pacific trade wind increase and Walker circulation strengthening were partly driven by teleconnections from Atlantic SST warming (McGregor et al., 2014; Chikamoto et al., 2015).

Interestingly, we find that W-CLIM high-season Amazon discharge is significantly correlated with observations, though explaining only about half the variance as W-FULL (**Table 2**). Examination of the Amazon discharge time series reveals that much of the skill comes from decreases in 1983 and 1992 following the 1982 El Chichón and 1991 Mount Pinatubo eruptions (**Fig. 2e**). These W-CLIM decreases are consistent with findings of reduced Amazon streamflow following large tropical eruptions (Iles and Hegerl, 2015). The decrease magnitudes are smaller than W-FULL, which incorporates the Pacific trade wind anomalies related to the 1982–83 and 1991–92 El Niño events.

The Amazon region wet-season precipitation increase simulated in W-FULL is driven by increased moisture convergence via atmospheric dynamical changes, through a strengthened Walker circulation. However, within this large-scale framework, we note that the relatively low-resolution IPSL-CM5A-LR model does not directly simulate some of the convective-to-synoptic-scale features important for Amazon wet-season precipitation, such as coastal-generated squall lines (Greco et al., 1990; Garstang et al., 1998). More work is needed to investigate the role of these higher-resolution processes over the Amazon, for instance using dynamical downscaling (Ramos da Silva and Haas, 2016).

Biases in IPSL-CM5A-LR may account for some of the spatial discrepancies between the observed and modeled changes over the Amazon. The double ITCZ and excessive eastern Pacific cold tongue biases, common to many models (Li and Xie, 2014; Zhang et al., 2019), translate into too-weak southerly cross-equatorial winds (Hu and Fedorov, 2018) and may explain the spurious moisture advection trend from the equatorial Pacific in W-FULL. Some circulation differences may also stem from the model's coarse orographic representation of the Andes Mountains (Insel et al., 2010). Additional examination of *pacemaker*-type simulations such as those through the Decadal Climate Prediction Project (Boer et al., 2016) can help assess the robustness of our results in a multi-model framework.

There is insufficient tropical North Atlantic SST warming in our simulations, which may cause discrepancies in the equatorial Atlantic wind field and explain the lack of moisture advected by the model mean flow. The weak tropical North Atlantic warming may also account for W-FULL's lack of skill in simulating dry season (July–October) precipitation and low-season river discharge (**Table**

**S4, Fig. S6**), which are negatively associated with the tropical Atlantic interhemispheric SST contrast through the position of the ITCZ (Yoon and Zeng, 2010; Fernandes et al., 2015). The model could be missing the observed warming from declining North American and European sulfate aerosols (Cox et al., 2008; Hua et al., 2019), which do not vary in our simulations, or from increased ocean heat transport convergence to the tropical North Atlantic (Servain et al., 2014).

Despite these caveats, our study provides strong evidence for the influence of the tropical Pacific on the intensification of Amazon basin wet-season precipitation and high-season discharge from the early 1990s to the early 2010s. As the Amazon region faces increasing anthropogenic stressors over the coming decades, understanding the role of decadal ocean-atmosphere variability will be important to reduce uncertainties in climate-related hydrological impacts. For example, since around 2013, there has been a reversal in the tropical Pacific toward a positive IPO phase (Meehl et al., 2016; Cha et al., 2018). This would suggest decreased wet-season precipitation and high-season discharge, though the reductions may be limited compared to previous decades as continued tropical Atlantic warming dampens the interbasin SST contrast (Barichivich et al., 2018). Further comparative studies prescribing tropical Pacific wind stress could help in understanding the ongoing hydroclimate changes in the vital Amazon region.

**Acknowledgments**

A.R.F. was supported by the UK NERC-funded SMURPHs project (NE/N006143/1). A.R.F, G.G, and M.K were also supported by the French ANR under the program Facing Societal, Climate and Environmental Changes (MORDICUS project, Grant ANR-13-SENV-0002). This work was granted access to the HPC resources of TGCC under the allocation 2015-017403 and 2016-017403 made by GENCI. GPCP was produced as part of the GEWEX effort under the WCRP. The ERSST and GPCP data were provided by the NOAA/OAR/ESRL PSL, and ERA-Interim was provided by ECMWF and C3S. The Amazon discharge at Óbidos was provided by the SO HYBAM Amazon Basin Water Resources Observation Service monitoring network (www.so-hybam.org). We appreciate the constructive feedback from three anonymous reviewers.

**References**

Adler, R.F., Huffman, G.J., Chang, A., Ferraro, R., Xie, P.-P., Janowiak, J., Rudolf, B., Schneider, U., Curtis, S., Bolvin, D., Gruber, A., Susskind, J., Arkin, P., Nelkin, E., 2003. The Version-2 Global Precipitation Climatology Project (GPCP) Monthly Precipitation Analysis (1979–Present). J. Hydrometeorol. 4, 1147–1167. https://doi.org/10.1175/1525-7541(2003)004<1147:TVGPCP>2.0.CO;2

Adler, R.F., Sapiano, M.R.P., Huffman, G.J., Wang, J.-J., Gu, G., Bolvin, D., Chiu, L., Schneider, U., Becker, A., Nelkin, E., Xie, P., Ferraro, R., Shin, D.-B., 2018. The Global Precipitation Climatology Project (GPCP) Monthly Analysis (New Version 2.3) and a Review of 2017 Global Precipitation. Atmosphere 9, 138. https://doi.org/10.3390/atmos9040138

Andreoli, R.V., Souza, R.A.F. de, Kayano, M.T., Candido, L.A., 2012. Seasonal anomalous rainfall in the central and eastern Amazon and associated anomalous oceanic and atmospheric patterns. Int. J. Climatol. 32, 1193–1205. https://doi.org/10.1002/joc.2345

Angelini, I.M., Garstang, M., Davis, R.E., Hayden, B., Fitzjarrald, D.R., Legates, D.R., Greco, S., Macko, S., Connors, V., 2011. On the coupling between vegetation and the atmosphere. Theor. Appl. Climatol. 105, 243–261. https://doi.org/10.1007/s00704-010-0377-5

Arraut, J.M., Nobre, C., Barbosa, H.M.J., Obregon, G., Marengo, J., 2012. Aerial Rivers and Lakes: Looking at Large-Scale Moisture Transport and Its Relation to Amazonia and to Subtropical Rainfall in South America. J. Clim. 25, 543–556. https://doi.org/10.1175/2011JCLI4189.1

Balmaseda, M.A., Trenberth, K.E., Källén, E., 2013. Distinctive climate signals in reanalysis of global ocean heat content. Geophys. Res. Lett. 40, 1754–1759. https://doi.org/10.1002/grl.50382

Barichivich, J., Gloor, E., Peylin, P., Brienen, R.J.W., Schöngart, J., Espinoza, J.C., Pattnayak, K.C., 2018. Recent intensification of Amazon flooding extremes driven by strengthened Walker circulation. Sci. Adv. 4, eaat8785. https://doi.org/10.1126/sciadv.aat8785

Bellenger, H., Guilyardi, É., Leloup, J., Lengaigne, M., Vialard, J., 2014. ENSO representation in climate models: from CMIP3 to CMIP5. Clim. Dyn. 42, 1999–2018.

Boer, G.J., Smith, D.M., Cassou, C., Doblas-Reyes, F., Danabasoglu, G., Kirtman, B., Kushnir, Y., Kimoto, M., Meehl, G.A., Msadek, R., Mueller, W.A., Taylor, K.E., Zwiers, F., Rixen, M., Ruprich-Robert, Y., Eade, R., 2016. The Decadal Climate Prediction Project (DCPP) contribution to CMIP6. Geosci. Model Dev. 9, 3751–3777. https://doi.org/10.5194/gmd-9-3751-2016

Bretherton, C.S., Widmann, M., Dymnikov, V.P., Wallace, J.M., Bladé, I., 1999. The Effective Number of Spatial Degrees of Freedom of a Time-Varying Field. J. Clim. 12, 1990–2009. https://doi.org/10.1175/1520-0442(1999)012<1990:TENOSD>2.0.CO;2

Cha, S.-C., Moon, J.-H., Song, Y.T., 2018. A Recent Shift Toward an El Niño-Like Ocean State in the Tropical Pacific and the Resumption of Ocean Warming. Geophys. Res. Lett. 45, 11,885-11,894. https://doi.org/10.1029/2018GL080651

Chikamoto, Y., Timmermann, A., Luo, J.-J., Mochizuki, T., Kimoto, M., Watanabe, M., Ishii, M., Xie, S.-P., Jin, F.-F., 2015. Skilful multi-year predictions of tropical trans-basin climate variability. Nat. Commun. 6, 6869. https://doi.org/10.1038/ncomms7869

Clarke, A.J., 2008. introduction to the dynamics of El Niño and the southern oscillation. Academic.

Cox, P.M., Harris, P.P., Huntingford, C., Betts, R.A., Collins, M., Jones, C.D., Jupp, T.E., Marengo, J.A., Nobre, C.A., 2008. Increasing risk of Amazonian drought due to decreasing aerosol pollution. Nature 453, 212–215. https://doi.org/10.1038/nature06960

Dai, A., 2016. Historical and future changes in streamflow and continental runoff: A review. Chapter 2, 17–37.

Dai, A., Qian, T., Trenberth, K.E., Milliman, J.D., 2009. Changes in Continental Freshwater Discharge from 1948 to 2004. J. Clim. 22, 2773–2792. https://doi.org/10.1175/2008JCLI2592.1

Dai, A., Trenberth, K.E., 2002. Estimates of freshwater discharge from continents: Latitudinal and seasonal variations. J. Hydrometeorol. 3, 660–687. https://doi.org/10.1175/1525-7541(2002)003<0660:EOFDFC>2.0.CO;2

Dai, A., Wigley, T.M.L., 2000. Global patterns of ENSO-induced precipitation. Geophys. Res. Lett. 27, 1283–1286. https://doi.org/10.1029/1999GL011140

de Boisséson, E., Balmaseda, M.A., Abdalla, S., Källén, E., Janssen, P. a. E.M., 2014. How robust is the recent strengthening of the Tropical Pacific trade winds? Geophys. Res. Lett. 41, 4398–4405. https://doi.org/10.1002/2014GL060257

Dee, D.P., Uppala, S.M., Simmons, A.J., Berrisford, P., Poli, P., Kobayashi, S., Andrae, U., Balmaseda, M.A., Balsamo, G., Bauer, P., Bechtold, P., Beljaars, A.C.M., van de Berg, L., Bidlot, J., Bormann, N., Delsol, C., Dragani, R., Fuentes, M., Geer, A.J., Haimberger, L., Healy, S.B., Hersbach, H., Hólm, E.V., Isaksen, L., Kållberg, P., Köhler, M., Matricardi, M., McNally, A.P., Monge-Sanz, B.M., Morcrette, J. -J, Park, B. -K, Peubey, C., de Rosnay, P., Tavolato, C., Thépaut, J. -N, Vitart, F., 2011. The ERA-Interim reanalysis: configuration and performance of the data assimilation system. Q. J. R. Meteorol. Soc. 137, 553–597. https://doi.org/10.1002/qj.828

DiNezio, P.N., Clement, A.C., Vecchi, G.A., Soden, B.J., Kirtman, B.P., Lee, S.-K., 2009. Climate Response of the Equatorial Pacific to Global Warming. J. Clim. 22, 4873–4892. https://doi.org/10.1175/2009JCLI2982.1

Dong, B., Lu, R., 2013. Interdecadal enhancement of the walker circulation over the Tropical Pacific in the late 1990s. Adv. Atmospheric Sci. 30, 247–262. https://doi.org/10.1007/s00376-012-2069-9

Douville, H., Voldoire, A., Geoffroy, O., 2015. The recent global warming hiatus: What is the role of Pacific variability? Geophys. Res. Lett. 42, 2014GL062775. https://doi.org/10.1002/2014GL062775

Drumond, A., Marengo, J., Ambrizzi, T., Nieto, R., Moreira, L., Gimeno, L., 2014. The role of the Amazon Basin moisture in the atmospheric branch of the hydrological cycle: a Lagrangian analysis. Hydrol. Earth Syst. Sci. 18, 2577–2598. https://doi.org/10.5194/hess-18-2577-2014

Dufresne, J.-L., Foujols, M.-A., Denvil, S., Caubel, A., Marti, O., Aumont, O., Balkanski, Y., Bekki, S., Bellenger, H., Benshila, R., Bony, S., Bopp, L., Braconnot, P., Brockmann, P., Cadule, P., Cheruy, F., Codron, F., Cozic, A., Cugnet, D., Noblet, N. de, Duvel, J.-P., Ethé, C., Fairhead, L., Fichefet, T., Flavoni, S., Friedlingstein, P., Grandpeix, J.-Y., Guez, L., Guilyardi, E., Hauglustaine, D., Hourdin, F., Idelkadi, A., Ghattas, J., Joussaume, S., Kageyama, M., Krinner, G., Labetoulle, S., Lahellec, A., Lefebvre, M.-P., Lefevre, F., Levy, C., Li, Z.X., Lloyd, J., Lott, F., Madec, G., Mancip, M., Marchand, M., Masson, S., Meurdesoif, Y., Mignot, J., Musat, I., Parouty, S., Polcher, J., Rio, C., Schulz, M., Swingedouw, D., Szopa, S., Talandier, C., Terray, P., Viovy, N., Vuichard, N., 2013. Climate change projections using the IPSL-CM5 Earth System Model: from CMIP3 to CMIP5. Clim. Dyn. 40, 2123–2165. https://doi.org/10.1007/s00382-012-1636-1

England, M.H., McGregor, S., Spence, P., Meehl, G.A., Timmermann, A., Cai, W., Gupta, A.S., McPhaden, M.J., Purich, A., Santoso, A., 2014. Recent intensification of wind-driven circulation in the Pacific and the ongoing warming hiatus. Nat. Clim. Change 4, 222–227. https://doi.org/10.1038/nclimate2106

Fernandes, K., Giannini, A., Verchot, L., Baethgen, W., Pinedo-Vasquez, M., 2015. Decadal covariability of Atlantic SSTs and western Amazon dry-season hydroclimate in observations

and CMIP5 simulations. Geophys. Res. Lett. 42, 6793–6801. https://doi.org/10.1002/2015GL063911

Foley, J.A., Botta, A., Coe, M.T., Costa, M.H., 2002. El Niño–Southern oscillation and the climate, ecosystems and rivers of Amazonia. Glob. Biogeochem. Cycles 16, 79-1-79–20. https://doi.org/10.1029/2002GB001872

Frankignoul, C., Gastineau, G., Kwon, Y.-O., 2017. Estimation of the SST Response to Anthropogenic and External Forcing and Its Impact on the Atlantic Multidecadal Oscillation and the Pacific Decadal Oscillation. J. Clim. 30, 9871–9895. https://doi.org/10.1175/JCLI-D-17-0009.1

Garstang, M., White, S., Shugart, H.H., Halverson, J., 1998. Convective cloud downdrafts as the cause of large blowdowns in the Amazon rainforest. Meteorol. Atmospheric Phys. 67, 199–212. https://doi.org/10.1007/BF01277510

Gastineau, G., Friedman, A.R., Khodri, M., Vialard, J., 2020. Correction to: Global ocean heat content redistribution during the 1998–2012 Interdecadal Pacific Oscillation negative phase. Clim. Dyn. 55, 2311–2311. https://doi.org/10.1007/s00382-020-05368-2

Gastineau, G., Friedman, A.R., Khodri, M., Vialard, J., 2019. Global ocean heat content redistribution during the 1998–2012 Interdecadal Pacific Oscillation negative phase. Clim. Dyn. 53, 1187–1208. https://doi.org/10.1007/s00382-018-4387-9

Gloor, M., Barichivich, J., Ziv, G., Brienen, R., Schöngart, J., Peylin, P., Cintra, B.B.L., Feldpausch, T., Phillips, O., Baker, J., 2015. Recent Amazon climate as background for possible ongoing and future changes of Amazon humid forests. Glob. Biogeochem. Cycles 1384–1399. https://doi.org/10.1002/2014GB005080@10.1002/(ISSN)1944-9224.TRENDSDAR1

Gloor, M., Brienen, R.J.W., Galbraith, D., Feldpausch, T.R., Schöngart, J., Guyot, J.-L., Espinoza, J.C., Lloyd, J., Phillips, O.L., 2013. Intensification of the Amazon hydrological cycle over the last two decades. Geophys. Res. Lett. 40, 1729–1733. https://doi.org/10.1002/grl.50377

Gouveia, N.A., Gherardi, D.F.M., Aragão, L.E.O.C., 2019. The Role of the Amazon River Plume on the Intensification of the Hydrological Cycle. Geophys. Res. Lett. n/a. https://doi.org/10.1029/2019GL084302

Greco, S., Swap, R., Garstang, M., Ulanski, S., Shipham, M., Harriss, R.C., Talbot, R., Andreae, M.O., Artaxo, P., 1990. Rainfall and surface kinematic conditions over central Amazonia during ABLE 2B. J. Geophys. Res. Atmospheres 95, 17001–17014. https://doi.org/10.1029/JD095iD10p17001

Grimm, A.M., 2003. The El Niño Impact on the Summer Monsoon in Brazil: Regional Processes versus Remote Influences. J. Clim. 16, 263–280. https://doi.org/10.1175/1520-0442(2003)016<0263:TENIOT>2.0.CO;2

Guimberteau, M., Drapeau, G., Ronchail, J., Sultan, B., Polcher, J., Martinez, J.-M., Prigent, C., Guyot, J.-L., Cochonneau, G., Espinoza, J.C., Filizola, N., Fraizy, P., Lavado, W., Oliveira, E.D., Pombosa, R., Noriega, L., Vauchel, P., 2012. Discharge simulation in the sub-basins of the Amazon using ORCHIDEE forced by new datasets. Hydrol. Earth Syst. Sci. 16, 911–935. https://doi.org/10.5194/hess-16-911-2012

Guimberteau, M., Ducharne, A., Ciais, P., Boisier, J.P., Peng, S., De Weirdt, M., Verbeeck, H., 2014. Testing conceptual and physically based soil hydrology schemes against observations for the Amazon Basin. Geosci. Model Dev. 7, 1115–1136. https://doi.org/10.5194/gmd-7-1115-2014

Hegerl, G., Zwiers, F., 2011. Use of models in detection and attribution of climate change. Wiley Interdiscip. Rev. Clim. Change 2, 570–591. https://doi.org/10.1002/wcc.121

Hourdin, F., Foujols, M.-A., Codron, F., Guemas, V., Dufresne, J.-L., Bony, S., Denvil, S., Guez, L., Lott, F., Ghattas, J., others, 2013. Impact of the LMDZ atmospheric grid configuration on the climate and sensitivity of the IPSL-CM5A coupled model. Clim. Dyn. 40, 2167–2192.

Hu, S., Fedorov, A.V., 2018. Cross-equatorial winds control El Niño diversity and change. Nat. Clim. Change 8, 798–802. https://doi.org/10.1038/s41558-018-0248-0

Hua, W., Dai, A., Zhou, L., Qin, M., Chen, H., 2019. An Externally Forced Decadal Rainfall Seesaw Pattern Over the Sahel and Southeast Amazon. Geophys. Res. Lett. 46, 923–932. https://doi.org/10.1029/2018GL081406

Huang, B., Thorne, P.W., Banzon, V.F., Boyer, T., Chepurin, G., Lawrimore, J.H., Menne, M.J., Smith, T.M., Vose, R.S., Zhang, H.-M., 2017. NOAA Extended Reconstructed Sea Surface Temperature (ERSST), Version 5. https://doi.org/10.7289/V5T72FNM

Huang, P., 2014. Regional response of annual-mean tropical rainfall to global warming. Atmospheric Sci. Lett. 15, 103–109. https://doi.org/10.1002/asl2.475

Iles, C.E., Hegerl, G.C., 2015. Systematic change in global patterns of streamflow following volcanic eruptions. Nat. Geosci. 8, 838+. https://doi.org/10.1038/NGEO2545

Insel, N., Poulsen, C.J., Ehlers, T.A., 2010. Influence of the Andes Mountains on South American moisture transport, convection, and precipitation. Clim. Dyn. 35, 1477–1492. https://doi.org/10.1007/s00382-009-0637-1

Jahfer, S., Vinayachandran, P.N., Nanjundiah, R.S., 2017. Long-term impact of Amazon river runoff on northern hemispheric climate. Sci. Rep. 7, 10989. https://doi.org/10.1038/s41598-017-10750-y

Jones, C., Carvalho, L.M.V., 2013. Climate Change in the South American Monsoon System: Present Climate and CMIP5 Projections. J. Clim. 26, 6660–6678. https://doi.org/10.1175/JCLI-D-12-00412.1

Kerr, R.A., 2000. A North Atlantic Climate Pacemaker for the Centuries. Science 288, 1984–1985. https://doi.org/10.1126/science.288.5473.1984

Khodri, M., Izumo, T., Vialard, J., Janicot, S., Cassou, C., Lengaigne, M., Mignot, J., Gastineau, G., Guilyardi, E., Lebas, N., Robock, A., McPhaden, M.J., 2017. Tropical explosive volcanic eruptions can trigger El Niño by cooling tropical Africa. Nat. Commun. 8, 778. https://doi.org/10.1038/s41467-017-00755-6

Kosaka, Y., Xie, S.-P., 2013. Recent global-warming hiatus tied to equatorial Pacific surface cooling. Nature 501, 403–407. https://doi.org/10.1038/nature12534

Krinner, G., Viovy, N., de Noblet-Ducoudré, N., Ogée, J., Polcher, J., Friedlingstein, P., Ciais, P., Sitch, S., Prentice, I.C., 2005. A dynamic global vegetation model for studies of the coupled atmosphere-biosphere system. Glob. Biogeochem. Cycles 19, GB1015. https://doi.org/10.1029/2003GB002199

Li, G., Xie, S.-P., 2014. Tropical Biases in CMIP5 Multimodel Ensemble: The Excessive Equatorial Pacific Cold Tongue and Double ITCZ Problems. J. Clim. 27, 1765–1780. https://doi.org/10.1175/JCLI-D-13-00337.1

Liu, B., Zhou, T., 2017. Atmospheric footprint of the recent warming slowdown. Sci. Rep. 7, 40947. https://doi.org/10.1038/srep40947

Ma, J., Xie, S.-P., 2013. Regional Patterns of Sea Surface Temperature Change: A Source of Uncertainty in Future Projections of Precipitation and Atmospheric Circulation. J. Clim. 26, 2482–2501. https://doi.org/10.1175/JCLI-D-12-00283.1

Madec, G., 2008. NEMO ocean engine [WWW Document]. URL http://nora.nerc.ac.uk/164324/ (accessed 4.12.16).

Malhi, Y., Roberts, J., Betts, R., Killeen, T., Li, W., Nobre, C., 2008. Climate change, deforestation, and the fate of the Amazon. SCIENCE 319, 169–172. https://doi.org/10.1126/science.1146961

Marengo, J.A., 2005. Characteristics and spatio-temporal variability of the Amazon River Basin Water Budget. Clim. Dyn. 24, 11–22. https://doi.org/10.1007/s00382-004-0461-6

Marengo, J.A., Espinoza, J.C., 2016. Extreme seasonal droughts and floods in Amazonia: causes, trends and impacts. Int. J. Climatol. 36, 1033–1050. https://doi.org/10.1002/joc.4420

Marengo, J.A., Liebmann, B., Grimm, A.M., Misra, V., Silva Dias, P.L., Cavalcanti, I.F.A., Carvalho, L.M.V., Berbery, E.H., Ambrizzi, T., Vera, C.S., Saulo, A.C., Nogues-Paegle, J., Zipser, E., Seth, A., Alves, L.M., 2012. Recent developments on the South American monsoon system. Int. J. Climatol. 32, 1–21. https://doi.org/10.1002/joc.2254

Marengo, J.A., Souza, C.M.J., Thonicke, K., Burton, C., Halladay, K., Betts, R.A., Alves, L.M., Soares, W.R., 2018. Changes in Climate and Land Use Over the Amazon Region: Current and Future Variability and Trends. Front. Earth Sci. 6. https://doi.org/10.3389/feart.2018.00228

McGregor, S., Timmermann, A., Stuecker, M.F., England, M.H., Merrifield, M., Jin, F.-F., Chikamoto, Y., 2014. Recent Walker circulation strengthening and Pacific cooling amplified by Atlantic warming. Nat. Clim. Change 4, 888–892. https://doi.org/10.1038/nclimate2330

Meehl, G.A., Arblaster, J.M., Fasullo, J.T., Hu, A., Trenberth, K.E., 2011. Model-based evidence of deep-ocean heat uptake during surface-temperature hiatus periods. Nat. Clim. Change 1, 360–364. https://doi.org/10.1038/NCLIMATE1229

Meehl, G.A., Hu, A., Teng, H., 2016. Initialized decadal prediction for transition to positive phase of the Interdecadal Pacific Oscillation. Nat. Commun. 7, 1–7. https://doi.org/10.1038/ncomms11718

Molinier, M., Guyot, J.-L., Oliveira, E. de, Guimaraes, V., 1996. Les régimes hydrologiques de l'Amazone et de ses affluents, in: Chevallier, P., Pouyaud, B. (Eds.), L'hydrologie tropicale : géosciences et outil pour le développement : mélanges à la mémoire de Jean Rodier, Publication - AISH. AISH, Wallingford, pp. 209–222.

Nobre, C.A., Sampaio, G., Borma, L.S., Castilla-Rubio, J.C., Silva, J.S., Cardoso, M., 2016. Land-use and climate change risks in the Amazon and the need of a novel sustainable development paradigm. Proc. Natl. Acad. Sci. 113, 10759–10768. https://doi.org/10.1073/pnas.1605516113

Oudar, T., Kushner, P.J., Fyfe, J.C., Sigmond, M., 2018. No Impact of Anthropogenic Aerosols on Early 21st Century Global Temperature Trends in a Large Initial-Condition Ensemble. Geophys. Res. Lett. 45, 9245–9252. https://doi.org/10.1029/2018GL078841

Power, S., Casey, T., Folland, C., Colman, A., Mehta, V., 1999. Inter-decadal modulation of the impact of ENSO on Australia. Clim. Dyn. 15, 319–324. https://doi.org/10.1007/s003820050284

Ramos da Silva, R., Haas, R., 2016. Ocean Global Warming Impacts on the South America Climate. Front. Earth Sci. 4. https://doi.org/10.3389/feart.2016.00030

Ropelewski, C.F., Halpert, M.S., 1987. Global and Regional Scale Precipitation Patterns Associated with the El Niño/Southern Oscillation. Mon. Weather Rev. 115, 1606–1626. https://doi.org/10.1175/1520-0493(1987)115<1606:GARSPP>2.0.CO;2

Santer, B.D., Wigley, T.M.L., Boyle, J.S., Gaffen, D.J., Hnilo, J.J., Nychka, D., Parker, D.E., Taylor, K.E., 2000. Statistical significance of trends and trend differences in layer-average atmospheric temperature time series. J. Geophys. Res. Atmospheres 105, 7337–7356. https://doi.org/10.1029/1999JD901105

Satyamurty, P., da Costa, C.P.W., Manzi, A.O., 2013a. Moisture source for the Amazon Basin: a study of contrasting years. Theor. Appl. Climatol. 111, 195–209. https://doi.org/10.1007/s00704-012-0637-7

Satyamurty, P., da Costa, C.P.W., Manzi, A.O., Candido, L.A., 2013b. A quick look at the 2012 record flood in the Amazon Basin. Geophys. Res. Lett. 40, 1396–1401. https://doi.org/10.1002/grl.50245

Servain, J., Caniaux, G., Kouadio, Y.K., McPhaden, M.J., Araujo, M., 2014. Recent climatic trends in the tropical Atlantic. Clim. Dyn. 43, 3071–3089. https://doi.org/10.1007/s00382-014-2168-7

Smith, D.M., Booth, B.B.B., Dunstone, N.J., Eade, R., Hermanson, L., Jones, G.S., Scaife, A.A., Sheen, K.L., Thompson, V., 2016. Role of volcanic and anthropogenic aerosols in the recent global surface warming slowdown. Nat. Clim. Change 6, 936.

Takahashi, C., Watanabe, M., 2016. Pacific trade winds accelerated by aerosol forcing over the past two decades. Nat. Clim. Change advance online publication. https://doi.org/10.1038/nclimate2996

Taylor, K.E., Stouffer, R.J., Meehl, G.A., 2012. An Overview of CMIP5 and the Experiment Design. Bull. Am. Meteorol. Soc. 93, 485–498. https://doi.org/10.1175/BAMS-D-11-00094.1

Vecchi, G.A., Soden, B.J., 2007. Global Warming and the Weakening of the Tropical Circulation. J. Clim. 20, 4316–4340.

Wang, C., 2006. An overlooked feature of tropical climate: Inter-Pacific-Atlantic variability. Geophys. Res. Lett. 33. https://doi.org/10.1029/2006GL026324

Wang, X.-Y., Li, X., Zhu, J., Tanajura, C.A.S., 2018. The strengthening of Amazonian precipitation during the wet season driven by tropical sea surface temperature forcing. Environ. Res. Lett. 13, 094015. https://doi.org/10.1088/1748-9326/aadbb9

Watanabe, M., Shiogama, H., Tatebe, H., Hayashi, M., Ishii, M., Kimoto, M., 2014. Contribution of natural decadal variability to global warming acceleration and hiatus. Nat. Clim. Change 4, 893. https://doi.org/10.1038/nclimate2355

Yin, L., Fu, R., Shevliakova, E., Dickinson, R.E., 2013. How well can CMIP5 simulate precipitation and its controlling processes over tropical South America? Clim. Dyn. 41, 3127–3143. https://doi.org/10.1007/s00382-012-1582-y

Yoon, J.-H., Zeng, N., 2010. An Atlantic influence on Amazon rainfall. Clim. Dyn. 34, 249–264. https://doi.org/10.1007/s00382-009-0551-6

Zhang, G.J., Song, X., Wang, Y., 2019. The double ITCZ syndrome in GCMs: A coupled feedback problem among convection, clouds, atmospheric and ocean circulations. Atmospheric Res. 229, 255–268. https://doi.org/10.1016/j.atmosres.2019.06.023

Zhang, Y., Wallace, J.M., Battisti, D.S., 1997. ENSO-like Interdecadal Variability: 1900–93. J. Clim. 10, 1004–1020. https://doi.org/10.1175/1520-0442(1997)010<1004:ELIV>2.0.CO;2

| | Observations | W-FULL | W-CLIM |
|---|---|---|---|
| **Dec–May Amazon precipitation** | 0.54 ± 0.41 mm day$^{-1}$ (GPCP) | 0.52 ± 0.28 mm day$^{-1}$ | –0.00 ± 0.06 mm day$^{-1}$ |
| **5-mon max Amazon discharge** | 15.2 ± 13.0 × $10^3$ m$^3$ s$^{-1}$ (Óbidos) | 34.4 ± 18.3 × $10^3$ m$^3$ s$^{-1}$ | –1.3 ± 4.5 × $10^3$ m$^3$ s$^{-1}$ |
| **Dec–May Pac–Atl ΔSST** | –0.55 ± 0.37 °C (ERSST) | –0.75 ± 0.45 °C | 0.03 ± 0.025 °C |

**Table 1. Wet-season trends**. 1992–2012 trends for observations and W-FULL and W-CLIM ensemble means, in decade$^{-1}$; mean slope and 95% confidence intervals. Top: December–May mean Amazon region (75°–50°W, 12.5°S–5°N) precipitation. Middle: mean high-season (5 largest months) Amazon river discharge. Bottom: December–May mean Pacific–Atlantic interbasin SST contrast (tropical central and eastern Pacific (180°–90°W, 10°S–10°N) minus tropical Atlantic (40°W–15°E, 10°S–10°N) SST).

| | W-FULL | W-CLIM |
|---|---|---|
| **Dec–May Amazon precipitation (GPCP)** | 0.72* | 0.32 |
| **5-mon max Amazon discharge (Óbidos)** | 0.57* | 0.41* |
| **Dec–May Pac–Atl ΔSST (ERSST)** | 0.90* | 0.05 |

**Table 2. Wet-season interannual correlations**. 1980–2014 detrended correlations of observations with W-FULL and W-CLIM ensemble means. Asterisks indicate statistically significant correlations at the 95% confidence level. Top: December–May mean Amazon region (75°–50°W, 12.5°S–5°N) precipitation. Middle: mean high-season (5 largest months) Amazon river discharge. Bottom: December–May mean Pacific–Atlantic interbasin SST contrast (tropical central and eastern Pacific (180°–90°W, 10°S–10°N) minus tropical Atlantic (40°W–15°E, 10°S–10°N) SST).

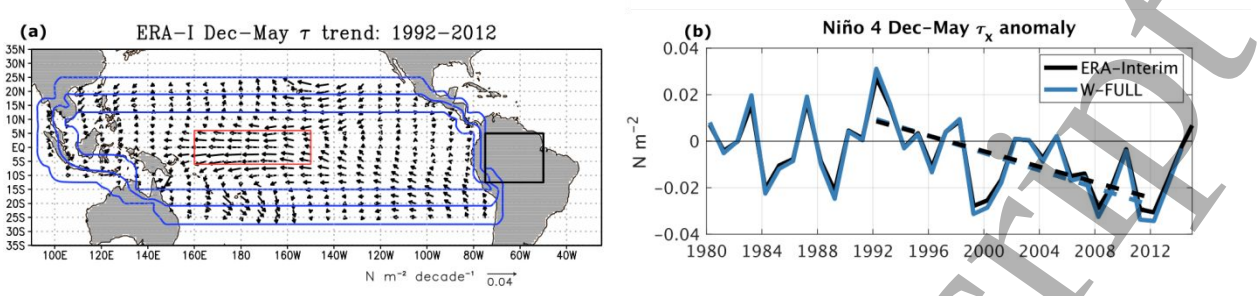


**Figure 1. Observed Pacific surface wind stress anomalies applied in nudging experiments**. (a) 1992–2012 December–May mean ERA-I wind stress trend ($\tau$) over the nudging mask region, in N m$^{-2}$ decade$^{-1}$. The blue contour intervals indicate regions of 0, 50, and 100% blending of model and nudged wind stress. The small red box outlines the Niño 4 region, and the black box outlines the Amazon precipitation region. (b) December–May mean zonal wind stress ($\tau_x$) anomaly over Niño 4 (160°E–150°W, 6°S–6°N) from ERA-I and applied in W-FULL, in N m$^{-2}$. Anomalies are computed from the 1980–1992 climatology; dashed line indicates the 1992–2012 linear trend.

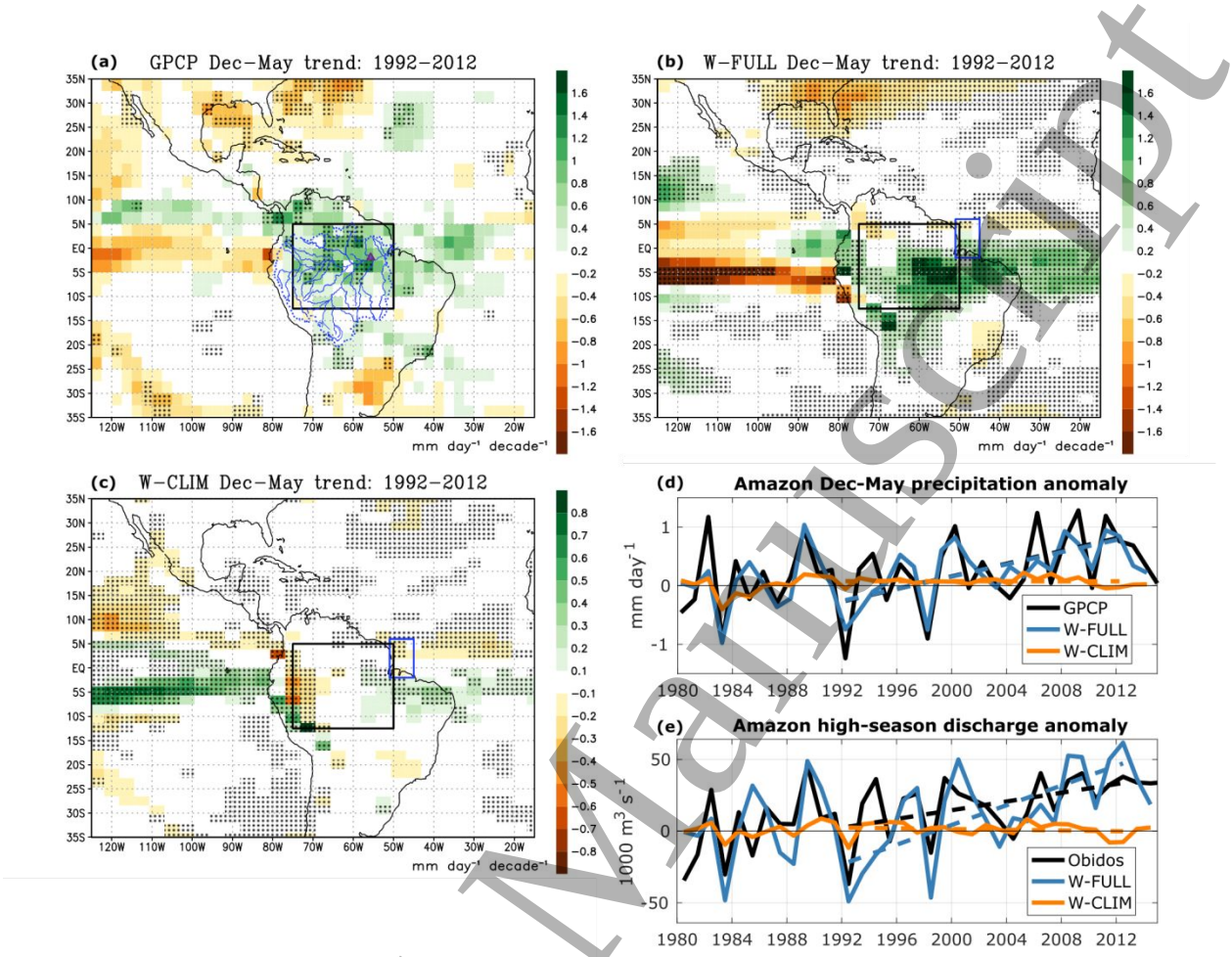


**Figure 2. Amazon basin wet-season precipitation and high-season river discharge**. (a–c) 1992-2012 December–May mean precipitation trend, in mm day$^{-1}$ decade$^{-1}$: (a) GPCP, (b) W-FULL, and (c) W-CLIM (note doubled color scale). Stippled regions are significant at $p<0.05$. The large black box outlines the Amazon precipitation region. In (a), the Amazon drainage basin and river system are indicated by the dotted black and solid blue lines respectively, and the purple triangle shows the Óbidos gauge station. In (b-c), the small blue box indicates the region where freshwater flux is integrated to calculate Amazon river discharge. (d) December–May mean Amazon region (75°–50°W, 12.5°S–5°N) precipitation anomaly for GPCP, W-FULL, and W-CLIM, in mm day$^{-1}$. (e) Mean high-season (5 largest months) Amazon river discharge anomaly from Óbidos, W-FULL, and W-CLIM, in $10^3$ m$^3$ s$^{-1}$. Anomalies in (d-e) are computed from the 1980–1992 climatology; dashed lines indicate the 1992–2012 linear trend.

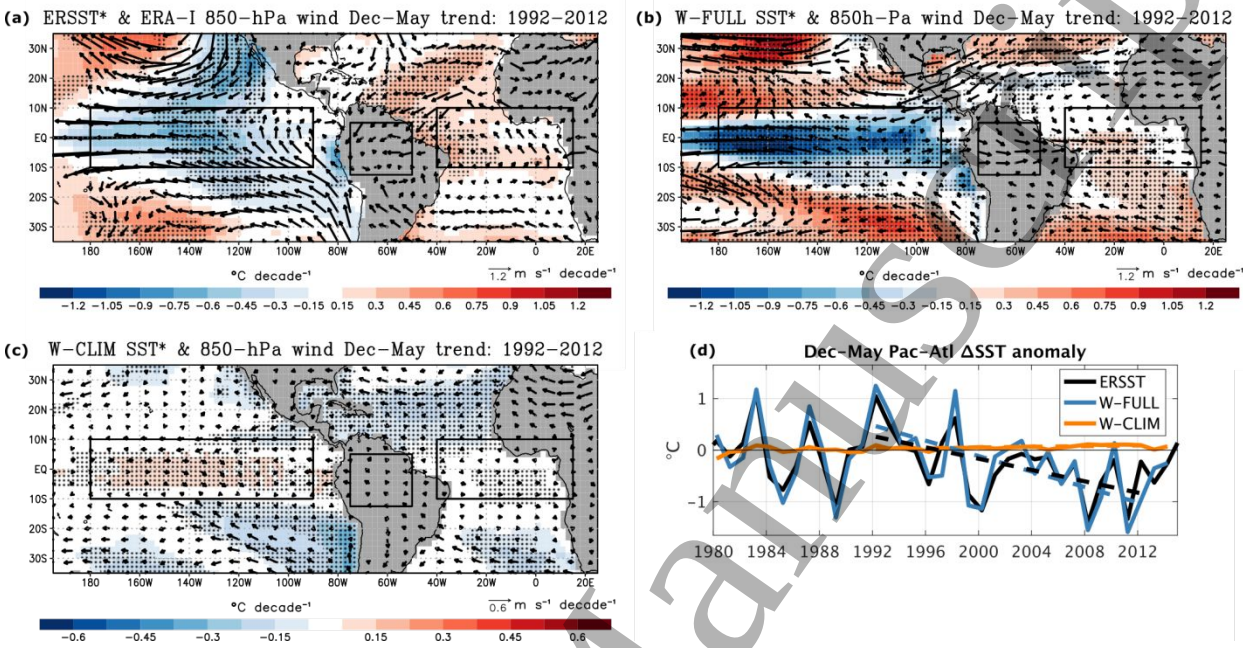


**Figure 3. Relative SST, low-level atmospheric circulation, and interbasin contrast.** (a–c) 1992–2012 December–May mean trend in relative SST (SST*, in °C decade$^{-1}$) and 850-hPa wind (in m s$^{-1}$ decade$^{-1}$): (a) ERSST and ERA-I, (b) W-FULL, and (c) W-CLIM (note doubled color and wind scales). Stippled regions are significant at $p<0.05$. Ocean boxes show the regions used to construct Pac–Atl ΔSST: the tropical central and eastern Pacific (180°–90°W, 10°S–10°N) and tropical Atlantic (40°W–15°E, 10°S–10°N). (d) December–May mean Pacific–Atlantic interbasin SST contrast anomaly (Pac–Atl ΔSST), in °C. Anomalies in (d) are computed from the 1980–1992 climatology; dashed lines indicate the 1992–2012 linear trend.

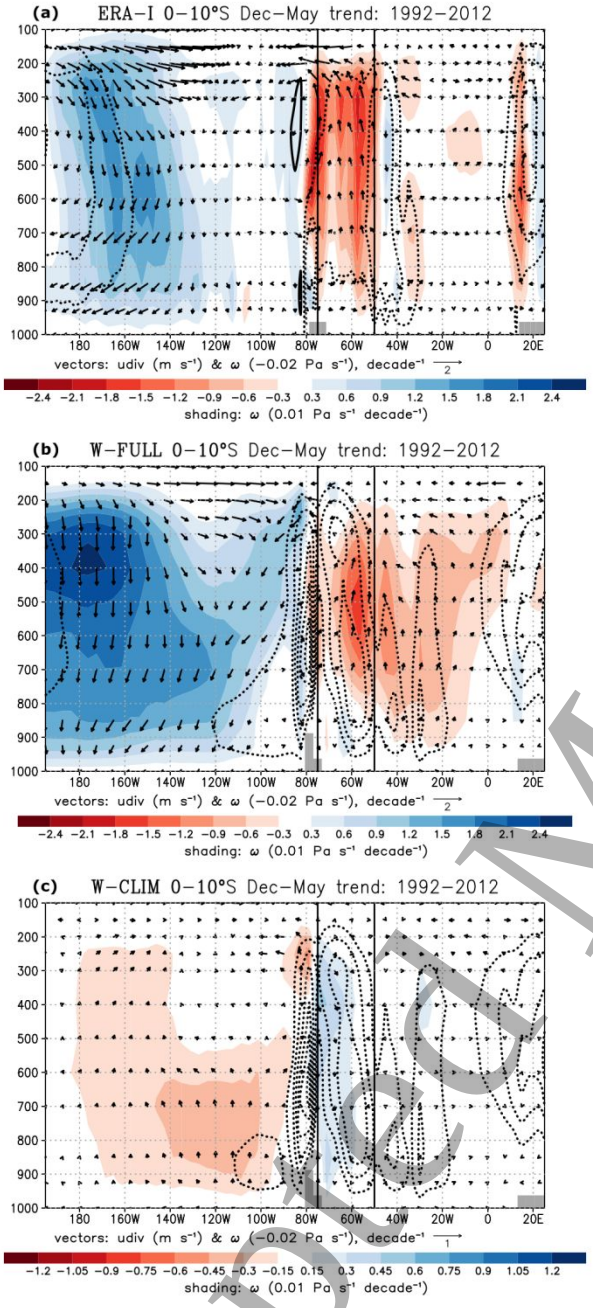


**Figure 4. Equatorial atmospheric zonal circulation**. 1992–2012 trends in December–May meridionally-averaged 0–10°S pressure vertical velocity (ω, in Pa $s^{-1}$ $decade^{-1}$) and divergent zonal wind ($u_{div}$, in m $s^{-1}$ $decade^{-1}$). Shading shows trends in ω, and vectors show trends in ω and $u_{div}$: (a) ERA-I, (b) W-FULL, and (c) W-CLIM (note doubled color and wind scales). The ω vector component is multiplied by a factor of –50. Contours show the 1980–1992 December–May mean ω climatology: solid contours show positive values, dashed contours show negative values; the contour interval is 0.02 Pa $s^{-1}$; and the zero contour is omitted. Vertical lines at 75° and 50°W outline the Amazon region.